ARTICLE

Discovery of piperidine-substituted thiazolo[5,4-d] pyrimidine derivatives as potent and orally bioavailable HIV-1 non-nucleoside reverse transcriptase inhibitors

Dongwei Kang [1], Tong Zhao[1], Zhao Wang[1], Da Feng[1], Heng Zhang[1], Boshi Huang [1], Gaochan Wu[1], Fenju Wei[1], Zhongxia Zhou[1], Lanlan Jing[1], Xiaofang Zuo[1], Ye Tian[1], Vasanthanathan Poongavanam [2], Jacob Kongsted [2], Erik De Clercq [3], Christophe Pannecouque[3], Peng Zhan[1] & Xinyong Liu[1]

HIV-1 reverse transcriptase offers a key target for antiviral therapy. However, the rapid emergence of drug-resistant mutations in reverse transcriptase as well as the poor pharmacokinetic properties of HIV-1 non-nucleoside reverse transcriptase inhibitors (NNRTIs) limits their clinical use. Starting from a previous piperidine-substituted thiophene[3,2-d] pyrimidine compound (K-5a2), here we explore the chemical space around the thiophene ring located in the solvent-exposed regions of the NNRTI binding pocket in detail. Bioisosterism-based structural modification leads to the discovery of a number of compounds as potent in vitro reverse transcriptase inhibitors, providing improved drug resistance profiles compared to the listed drug Etravirine. Furthermore, **14a** and **19a** are identified as lead compounds with good solubility, appropriate ligand efficiency, and lower cytochrome P450 liability. Compound **19a** exhibits useful in vivo pharmacokinetic properties in rat and safety in mice, suggesting that it may have the potential to be an effective drug candidate for treating AIDS.

[1] Department of Medicinal Chemistry, Key Laboratory of Chemical Biology (Ministry of Education), School of Pharmaceutical Sciences, Shandong University, 44 West Culture Road, 250012 Jinan, Shandong, PR China. [2] Department of Physics, Chemistry, and Pharmacy, University of Southern Denmark, DK-5230 Odense M, Denmark. [3] Rega Institute for Medical Research, Laboratory of Virology and Chemotherapy, K.U. Leuven, Herestraat 49 Postbus 1043 (09.A097), B-3000 Leuven, Belgium. Correspondence and requests for materials should be addressed to C.P. (email: christophe.pannecouque@rega.kuleuven.be) or to P.Z. (email: zhanpeng1982@sdu.edu.cn) or to X.L. (email: xinyongl@sdu.edu.cn)

HIV-1 reverse transcriptase (RT) represents one of the most successful molecular targets for novel development of precise medicine to treat AIDS patients[1]. Two generations of non-nucleoside RT inhibitors (NNRTIs) have been awarded FDA approval[2]. The second-generation NNRTIs, Etravirine (ETV) and Rilpivirine (RPV) (Fig. 1), were designed to suppress most of the RT-resistant mutations caused by treatment of the first-generation NNRTIs, especially the K103N and Y181C mutation[3,4]. Although ETV and RPV exhibited higher genetic barriers to emergence of drug resistance, they generally failed to interact with the most refractory mutations E138K and RES056 (K103N + Y181C)[5,6]. In addition, hypersensitivity reactions or other adverse effects have been reported with second-generation NNRTIs[2,7].

Our previous efforts have led to the development of two novel NNRTIs **3** (K-5a2) and **4** (25a) with a piperidine-substituted thiophene[3,2-*d*]pyrimidine scaffold[8,9]. Both compounds exhibit highly potency toward wild-type (WT) strain and numerous clinically observed variants compared to ETV. However, the activity of **3** against the most challenging double mutation RES056 is inferior to that of ETV. Although **4** proved to be capable of inhibiting all of the resistant RT-mutants with single-nanomole activities, it also showed greater cytotoxicity (CC_{50} = 2.30 μM). This may be caused by the cyanovinyl group, as it can act as a Michael acceptor and potentially result in covalent modification of proteins and nucleic acids[10]. In addition, both **3** and **4** exhibit extremely low aqueous solubility, far below that of the typical range (4−4000 μg/mL) for oral drugs. The low solubility results in poor bioavailability of **3** ($F = 22.9\%$) and **4** ($F = 16.2\%$). This has prompted the search for novel HIV-1 inhibitors with improved drug resistance profiles and pharmacokinetic properties.

With the aim to provide valuable insights into the favorable structural features for further structure-based design, we have determined the crystal structures of HIV-1 WT and some mutant RT variants in complex with **3**. The co-crystal structures demonstrated that the hydrophobic interactions of the left wing, the network of the main chain of hydrogen bonds formed between the NNRTIs and NNRTIs binding pocket (NNIBP), and its structural flexibility all play important roles in maintaining its high potency against mutant strains. These high-resolution co-crystal structures illustrate the molecular details of the binding mode, and provide valuable insights into favorable structural features that can be employed for designing novel HIV-1 NNRTIs that are broadly active against drug-resistant HIV-1 RT variants[11].

The application of structural mimics of extensive scaffolds or peripheral substituents, commonly designated as bioisosteric replacement strategy, is a common approach in contemporary drug design and discovery. Guided by previous structural biology studies, we kept the hydrophobic interactions and hydrogen bonds unchanged and modified the thiophene[3,2-*d*]pyrimidine core ring to the furo[3,2-*d*]pyrimidine and thiazolo[4,5-*d*]pyrimidine ring in the first round of the present study (Fig. 1). The rational is that the introduction of oxygen atom may develop novel hydrogen bonds (hydrogen bond receptor) with Glu138 in NNIBP. Moreover, the replacement of a CH moiety with a nitrogen atom in heteroaromatic ring systems can significantly alter the physicochemical properties and intra- and inter-molecular interactions, which may yield improved pharmacological and pharmacokinetics properties[12]. Following the disclosure of thiazolo[4,5-*d*]pyrimidine derivatives as potent HIV-1 inhibitors with potent activity against mutant HIV-1 strains RES056 in the first round, we also investigated the effects of substitution on the thiazolo[4,5-*d*]pyrimidine core to thiazolo[5,4-*d*]pyrimidine in the second round.

Here we report that the center ring can have dramatic effects on potency and pharmacokinetic properties. Especially, the compound **19a** is shown to exhibit favorable in vivo pharmacokinetic properties in rat and safety in mice, suggesting that it may lead to an effective drug candidate for treating AIDS.

Results

Synthesis and characterization of the target compounds. The designed library and synthesis were based on our previously reported methods[8] and are described in Fig. 2 and Supplementary Figs. 1, 2. 2,4-Dichlorofuro[3,2-*d*]pyrimidine (**5**) was selected as the starting material and was reacted with 4-hydroxy-3,5-dimethylbenzonitrile to yield intermediate **6**. Then nucleophilic substitution of **6** with 4-(*tert*-butoxycarbonyl)-aminopiperidine was conducted in the presence of potassium carbonate, and the product was subsequently treated with trifluoroacetic acid to provide the key intermediate **8**. Then target compounds **9a–f** were obtained by another nucleophilic substitution between **8** and 4-picolyl chloride hydrochloride or substituted benzyl chloride (or bromine). The synthetic procedures of **14a–f** and **19a–f** were similar to that of **9a–f**, only with the difference that 5,7-dichlorothiazolo[4,5-*d*]pyrimidine and 5,7-dichlorothiazolo[5,4-*d*]pyrimidine were used as starting materials (Supplementary Figs. 1, 2).

In vitro assay of anti-HIV activities in MT-4 cells. The newly designed derivatives **9a–f** and **14a–f** were evaluated for their activity against WT HIV-1 (IIIB), the most challenging double mutant HIV-1 strain RES056, and a HIV-2 strain (ROD) in the MT4 cell line. ETV was selected as control drug. The values of EC_{50} (anti-HIV potency), CC_{50} (cytotoxicity), SI (selectivity index, CC_{50}/EC_{50} ratio), and RF (fold-resistance factor, EC_{50} (mutant strains)/EC_{50} (WT strain)) of the target compounds were summarized.

As depicted in Table 1, ten of the newly synthesized twelve compounds showed high potency against the WT HIV-1 strain with low nanomolar EC_{50} values ranging from 1.1 to 3.4 nM, which are superior to that of the reference drug ETV (EC_{50} = 5.1 nM). In the case of double mutant HIV-1 strain RES056, **9a–f** with furo[3,2-*d*]pyrimidine scaffold showed a marked decrease of potency and **9d** turned out to be the most potent inhibitor with an EC_{50} value of 100.2 nM, but still being inferior to that of ETV (EC_{50} = 45.4 nM). Among the derivatives in sub-series **14** with the thiazolo[4,5-*d*]pyrimidine scaffold, **14a**, **14c**, and **14d** could potently inhibit RES056 with EC_{50} values of 26.1, 27.4 and 24.7 nM respectively, being about twofold more potent than ETV. Moreover, **14a** and **14d** also demonstrated with lower cytotoxicity (CC_{50} = 25.1 and 30.3 μM, respectively) and higher SI values toward WT (SI = 11071 and 16818) and mutant HIV-1 strains (SI = 961 and 1227).

Considering that the compounds of sub-series **14** with thiazolo[4,5-*d*]pyrimidine scaffold exhibited more active potency than compounds of sub-series **9** with furo[3,2-*d*]pyrimidine scaffold, we further replaced the thiazolo[4,5-*d*]pyrimidine with thiazolo[5,4-*d*]pyrimidine utilizing the bioisosterism strategy, with the aim to achieve more active potency against the double mutant strain RES056. As shown in Table 1, all the novel compounds were demonstrated with single-nanomole activity against WT HIV-1 strain. Moreover, **19a–d** exhibited more potent activity against RES056 than ETV, with EC_{50} values from 18.1 to 28.1 nM. Among them, **19a** (EC_{50} = 18.3 nM) and **19c** (EC_{50} = 18.1 nM) were the most potent inhibitors against RES056, being about 2-fold potent than that of ETV. All the results confirmed that the thiazolo[5,4-*d*]pyrimidine scaffold was favorable for improving the activity against RES056.
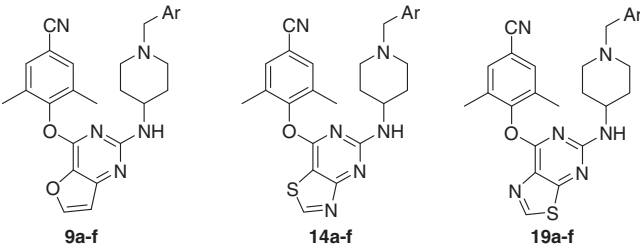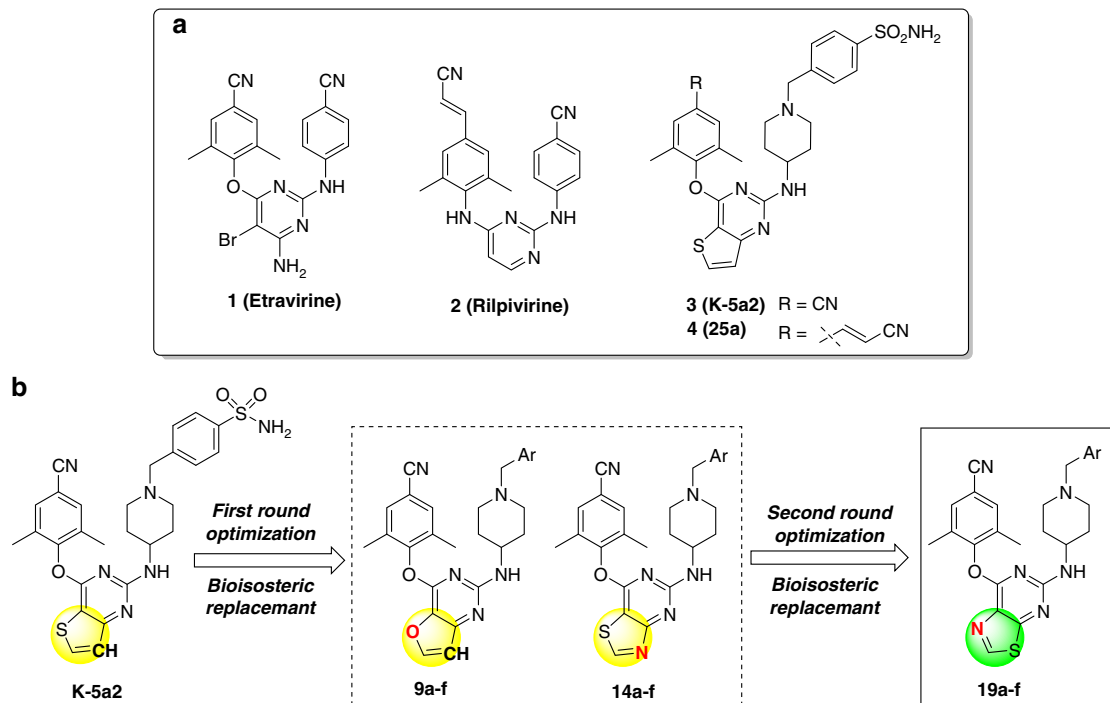
Fig. 1 Chemical structures of the leads and the design strategy in this study. **a** The chemical structures of the second-generation NNRTIs Etravirine (ETV), Rilpivirine (RPV) and our previously reported lead compounds K-5a2 **3** and 25a **4**. **b** Further optimization of the lead K-5a2 via bioisosteric replacement strategy. The yellow/green parts highlight the structural modifications of the central scaffold
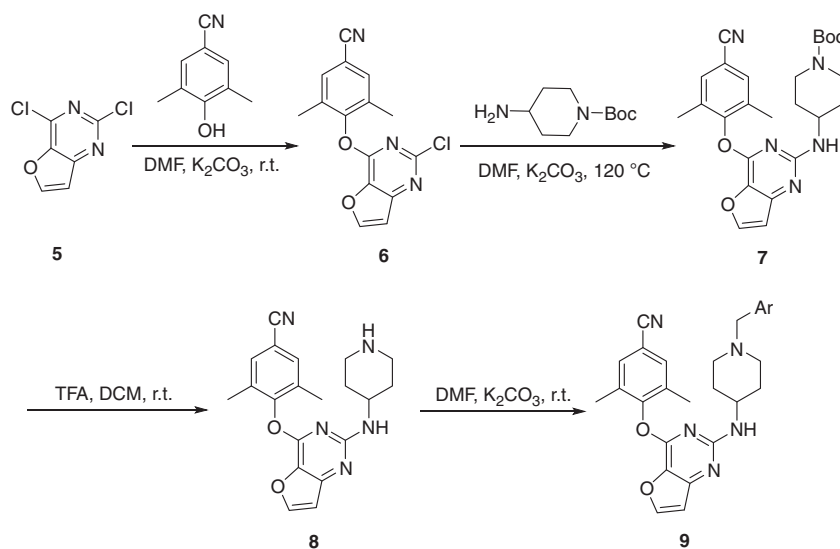
Fig. 2 The synthetic route of **9a–f**. Full details can be found in the Supplementary Methods

The structure-activity relationship (SARs) could be concluded clearly from their activities. Detailed comparison of the activities of **9a–d** vs **9e**, **14a–d** vs **14e**, and **19a–d** vs **19e** indicated that hydrophilic substituents harboring hydrogen bond donors or acceptors (Ar = 4-SO$_2$NH$_2$-Ph, 4-SO$_2$CH$_3$-Ph, 4-CO$_2$NH$_2$-Ph, and pyridine-4-yl) at the 4-position in the phenyl ring of the Ar could strengthen the interaction with the NNRTI binding site compared to hydrophobic substituent (Ar = 4-NO$_2$-Ph). Meanwhile, nitro-substitution-bearing compounds showed increased cytotoxicity compared to other hydrophilic substituted compounds, such as the CC$_{50}$ values of **9e**, **14e** and **19e** can up to

5.24, 5.17, and 5.68 μM, respectively. In addition, pairwise comparison of the activities of compounds **9b** vs **9 f** and **19b** vs **19 f** confirmed the critical role of the *para*-substitution in improving the activity against RES056 over *meta*-substitution. Moreover, comparison of the activities of sub-series **9**, sub-series **14** and sub-series **19** leads to the conclusion that the activity of compounds toward mutant strain RES056 were also greatly influenced by their central scaffolds, thiazolo[5,4-*d*]pyrimidine and thiazolo[4,5-*d*]pyrimidine display significantly improved drug resistance profiles, which were superior to that of furo [3,2-*d*]pyrimidine. It is well to be reminded that compound **14b**

Table 1 Anti-HIV activity evaluation of the target compounds

9a-f   14a-f   19a-f

Compounds	Ar	EC$_{50}$ (nM)		EC$_{50}$ (μM)	CC$_{50}$ (μM)	SI	
		IIIB	RES056	ROD		IIIB	RES056
9a	4-SO$_2$NH$_2$-Ph	1.5 ± 0.1327	112 ± 22.1709	>10.5468	10.5 ± 1.8475	6609	93
9b	4-CONH$_2$-Ph	1.7 ± 0.1424	187 ± 4.8415	8.66 ± 0.1392	26.7 ± 0.1947	15624	143
9c	4-SO$_2$CH$_3$-Ph	1.5 ± 0.2660	175 ± 38.5721	>4.3252	4.32 ± 1.3333	2874	25
9d	pyridine-4-yl	1.5 ± 0.3111	100 ± 24.1132	8.25 ± 0.5675	24.3 ± 3.9925	15785	243
9e	4-NO$_2$-Ph	5.9 ± 0.8250	911 ± 169.2097	>5.2487	5.24 ± 0.1857	880	6
9 f	3-CONH$_2$-Ph	1.1 ± 0.1424	879 ± 22.3565	>17.2343	17.2 ± 0.9109	15560	20
14a	4-SO$_2$NH$_2$-Ph	2.2 ± 0.9005	26.1 ± 1.5437	6.30 ± 2.3241	25.1 ± 0.7493	11071	961
14b	4-CONH$_2$-Ph	>15560	>15560	>15560	15.5 ± 2.8429	<1	<1
14c	4-SO$_2$CH$_3$-Ph	2.2 ± 0.6444	27.4 ± 0.3866	≥5.6134	10.9 ± 2.7502	4816	400
14d	pyridine-4-yl	1.8 ± 0.4498	24.7 ± 1.9493	6.11 ± 2.8123	30.3 ± 0.7605	16818	1227
14e	4-NO$_2$-Ph	3.4 ± 0.2743	128 ± 4.5258	>5.1753	5.17 ± 0.1343	1482	40
14 f	3-CONH$_2$-Ph	1.3 ± 0.0000	558 ± 8.5356	>27.3923	27.3 ± 0.9654	20099	49
19a	4-SO$_2$NH$_2$-Ph	1.6 ± 0.2572	18.3 ± 2.3156	3.11 ± 0.4502	23.2 ± 1.7538	14194	1265
19b	4-CONH$_2$-Ph	1.6 ± 0.1377	28.1 ± 13.0788	3.37 ± 0.7035	27.1 ± 1.3023	16412	965
19c	4-SO$_2$CH3-Ph	2.3 ± 0.7588	18.1 ± 1.1599	6.06 ± 1.4359	14.3 ± 5.5085	6212	791
19d	pyridine-4-yl	2.7 ± 0.0000	26.8 ± 0.1499	4.45 ± 0.4648	28.7 ± 0.4899	10447	1074
19e	4-NO$_2$-Ph	8.2 ± 1.9811	125 ± 16.0460	>5.6823	5.68 ± 0.4235	687	45
19 f	3-CONH$_2$-Ph	3.0 ± 0.6884	222 ± 47.0835	>28.8642	28.8 ± 0.6346	9565	130
ETV	—	5.1 ± 0.8122	45.4 ± 15.5950		>4.59	>889	>101

EC$_{50}$ concentration of compound required to achieve 50% protection of MT-4 cell cultures against HIV-1-induced cytopathic, as determined by the MTT method, CC$_{50}$ concentration required to reduce the viability of mock-infected cell cultures by 50%, as determined by the MTT method, SI selectivity index, the ratio of CC$_{50}$/EC$_{50}$

(EC$_{50}$ > 15560 nM) exhibited sharply reduced activity, compared to the other derivatives, though they are structurally similar molecules. This seems to be another good example of an activity cliff[13,14], which may be related to the flexibility of the binding pocket and the induced-fit mechanism of the NNRTIs[8].

Furthermore, compounds **14a**, **14c–d** and **19a–d**, which exhibited high potency against WT and RES056 HIV-1 strains, were tested for their potency against a panel of NNRTI-resistant strains, including single-mutant strains L100I, K103N, Y181C, Y188L, E138K, and double-mutant strain F227L + V106A. The results are depicted in Table 2 and Supplementary Table 1. As for mutant HIV-1 strain L100I, **14c** turned out to be the most potent inhibitor with EC$_{50}$ value of 2.70 nM, being about 2.2-fold than that of ETV (EC$_{50}$ = 6.0 nM). In the case of K103N, Y181C, 188 L and E138K, **19b** yielded the most active potency (EC$_{50}$ = 1.6, 5.1, 7.2 and 5.2 nM, respectively), which is more active than that of ETV (EC$_{50}$ = 3.3 nM, 14.5 nM, 20.8 nM and 9.7 nM, respectively). Moreover, the other compounds also exhibited comparable activity as ETV toward these single mutant HIV-1 strains. Against F227L + V106A, **14a**, **14c**, and **19a–c** showed comparable potency (EC$_{50}$ = 15.2–20.3 nM) with ETV (EC$_{50}$ = 19.7 nM), while compounds **14d** and **19d** with pyridine-4-yl group at the Ar region exhibiting a decreased activity with EC$_{50}$ values of 32.9 and 30.9 nM, respectively. This indicates that a pyridine-4-yl group at the Ar position is unable to maintain compounds activity toward resistance variants F227L + V106A effectively.

Recombinant HIV-1 reverse transcriptase inhibitory assays. To validate the binding target, some potent compounds were evaluated for their ability to inhibit recombinant WT HIV-1 RT enzyme. As shown in Table 3, all the selected compounds displayed highly inhibitory activity with IC$_{50}$ values of 0.037–0.050 μM, which were superior to that of EFV (IC$_{50}$ = 0.181 μM) and keep the same magnitude with that of ETV (IC$_{50}$ = 0.011 μM). The results confirmed the viewpoint that the newly synthesized derivatives showed high affinity to HIV-1 RT and acted as classical NNRTIs. However, the results demonstrated that the antiviral activities of these compounds were inconsistent with their RT inhibitory potencies. These differences are considered to be due to template-specific variation in the relationship between HIV-RT-RNA binding affinity and polymerase processivity and have been observed in most NNRTI series.

Molecular modeling studies. In a previous study, we crystalized HIV-1 RT complexes with the **K-5a2** ligand[15] which is very similar to the **14a**, **19a**, and **19c** compounds. Here, we consider prediction of the binding modes of these compounds through molecular modeling studies in different mutants. Molecular docking followed by MM-GBSA simulations were performed for **14a**, **19a**, and **19c** in eight mutants and WT. From several studies, the NNIBP is well characterized as being more hydrophobic and comprises of amino acids L100, V106, T107, V108, V179, Y181, Y188, G190, F227, W229, L234, and Y318[15,16]. Initially, the

Table 2 Activity against mutant HIV-1 strains of the preferred compounds

Compounds	EC$_{50}$ (nM)					
	L100I	K103N	Y181C	Y188L	E138K	F227L + V106A
14a	7.8 ± 0.2573	3.9 ± 1.9296	6.7 ± 1.2864	11.4 ± 2.3156	6.5 ± 1.5437	18.8 ± 4.5025
14c	3.2 ± 0.7733	3.8 ± 2.8352	7.0 ± 0.9021	10.7 ± 0.0000	6.1 ± 1.1599	15.4 ± 2.3197
14d	5.6 ± 2.2492	1.9 ± 0.5997	5.8 ± 2.2492	7.7 ± 1.0496	5.5 ± 1.1996	32.9 ± 23.8411
19a	9.6 ± 1.5437	1.9 ± 0.1286	6.5 ± 1.0291	10.8 ± 0.6432	7.9 ± 0.1286	16.0 ± 4.6311
19b	6.3 ± 2.8911	1.6 ± 0.4130	5.1 ± 0.1377	7.2 ± 0.2753	5.2 ± 0.8260	20.3 ± 2.6158
19c	5.6 ± 0.7733	3.3 ± 0.3866	7.5 ± 0.6444	7.1 ± 0.2578	6.6 ± 0.1289	15.2 ± 3.4796
19d	13.7 ± 7.1973	3.3 ± 2.3991	5.8 ± 0.1499	6.6 ± 1.0496	6.5 ± 0.2999	30.9 ± 6.2976
ETV	6.0 ± 1.5525	3.3 ± 0.6892	14.5 ± 8.2246	20.4 ± 8.6429	9.7 ± 6.9035	19.7 ± 7.3035

Table 3 Inhibitory activity against WT HIV-1 RT

Compounds	IC$_{50}$ (μM)	Compounds	IC$_{50}$ (μM)
14a	0.050 ± 0.010	**19a**	0.050 ± 0.001
14c	0.046 ± 0.003	**19c**	0.048 ± 0.003
14d	0.037 ± 0.001	**19d**	0.042 ± 0.003
NVP	0.181 ± 0.056	**ETV**	0.011 ± 0.000

IC$_{50}$ inhibitory concentration of test compound required to inhibit biotin deoxyuridine triphosphate (biotin-dUTP) incorporation into WT HIV-1 RT by 50%

binding mode of **K-5a2** and **ETV** was compared in the WT. As expected, both compounds showed very similar binding pose (Supplementary Figs. 3, 4) and possess π-π interactions and hydrogen bonding with Trp229 and Lys101/Lys102 residues, respectively. In addition, compound **K-5a2** makes additional hydrogen bonding between sulfonamide and residues such as Lys104 and Val106. Subsequently, the binding mode of the compounds used in the modeling study were also investigated in various mutants, however, for clarity, only the highly potent compound **19a** is discussed. Figure 3 shows the best binding poses of **19a**.

Overall, **19a** showed the same binding mode as **K-5a2** and **ETV**. The sulfonamide group is involved in hydrogen bonding with Val106 (or Ala106) and Lys104 in all mutants, including when Val106 was mutated to Ala106. Interestingly, thiazolopyrimidine showed better interaction with the NNIBP hydrophobic residues as compared to ETV, and particularly when it is substituted with thiazolopyrimidine, it makes π-H interactions with Val179 in all the mutant structures. In most cases, the binding affinity of **19a** was not affected by mutations, except for double mutants. For instance, the binding affinity remains almost the same in the K103N mutant, due to complementary hydrogen bonding between Asn103 with one of the nitrogen atoms of the thioazolopyrimidine ring of **19a** as observed in Lys103.

Solubility and lipophilic efficiency. In order to verify the drug-like properties of the promising compounds, the physicochemical properties of **14a**, **14c**, **14d**, and **19a–d** were determined. All the selected compounds were tested for their solubility at three different pH values (7.4, 7.0, and 2.0) with HPLC methods. The results are shown in Table 4. All compounds exhibited good solubility at pH 2.0 ($S > 178.3$ μg/mL). Especially, their solubility have been greatly improved compared to K-5a2 and ETV at pH 7.0 and pH 7.4. Among them, **14d** has the best solubility ($S = 33.8$ μg/mL, pH = 7.0; $S = 30.7$ μg/mL, pH = 7.4). The results are in accord with the purpose of our design.

To further screen compounds with good physicochemical properties, seven compounds **14a**, **14c,d** and **19a–d** were

calculated their activity efficiency, including lipophilic efficiency (LE), ligand lipophilic efficiency (LLE), and ligand efficiency dependent lipophilicity (LELP), which are regarded as important metrics to measure the balance between in vitro activity and in vivo drug-like properties[17]. As depicted in Table 4, all the selected compounds satisfied the acceptable levels for LE and LLE (LE > 0.3 and LLE > 5)[18], which means these compounds could combine their lipophilicity and in vitro potency well. Moreover, **14a**, **14d**, **19a**, and **19c** were also demonstrated with appropriate LELP value (LELP < 10), supplying a possibility that these compounds have more favorable ADME profiles than the lead **K-5a2** and the approved drug **ETV**.

In vitro effects on CYP enzymatic inhibitory activity. The drug metabolism in vivo was mainly accomplished by the metabolizing enzymes in the liver, especially the cytochrome P450 (CYP450), which including CYP1A, CYP3A, CYP2C, and CYP2D6[19]. On the other hand, the drugs could also inhibit the activity of CYP450 and down-regulate the expression of their genes, which may lead to metabolism-mediated drug-drug interactions (DDI) when co-administration different drugs and cause side effects[20,21]. Among these CYP450 isozymes, CYP3A4M is a major xenobiotic metabolizing enzyme, and it contributes to the metabolism of approximately 50% of prescribed drugs[22]. Considering the activity of **14d** against double mutant strain F227L + V106A was inferior to that of ETV, so only the lead **14a**, **19a**, and **19c** were evaluated for their CYP drug metabolizing enzymatic inhibitory activity. As depicted in Table 5, **14a** and **19a** yield lower inhibitory activity to all tested CYP isozymes (CYP1A2, CYP2C9, CYP2C19, CYP2D6, and CYP3A4M) with higher IC$_{50}$ values (IC$_{50 > }$ 3 μM), suggesting that **14a** and **19a** are anticipated to have a favorable drug interaction profile with respect to key CYP isozymes. In addition, **19c** exhibited a moderate inhibitory activity to CYP3A4M with an IC$_{50}$ value of 2.78 μM, which demonstrated that **19c** has a strong CYP3A4 inhibition activity and may cause strong DDI.

Pharmacokinetic study. Considering the promising activities, favorable physiochemical properties and lower CYP enzymatic inhibitory activity of **14a** and **19a**, they were further evaluated for their pharmacokinetics (PK) profiles by Wistar rats PK models following intravenous (iv) and oral administration (po) (Table 6 and Supplementary Fig. 5). The results demonstrated that **14a** and **19a** showed a suitable clearance (CL = 10.2 and 16.3 L/h/kg, respectively) and half-life (T$_{1/2}$ = 2.01 and 0.93 h, respectively) for a single 2 mg/kg iv dose. Furthermore, after a single 20 mg/kg po dose of **14a** and **19a**, they reached the maximum concentration (T$_{max}$) at 0.90 and 2.8 h with a C$_{max}$ of 272 and 2982 ng/mL, respectively. Moreover, both of them displayed an acceptable oral
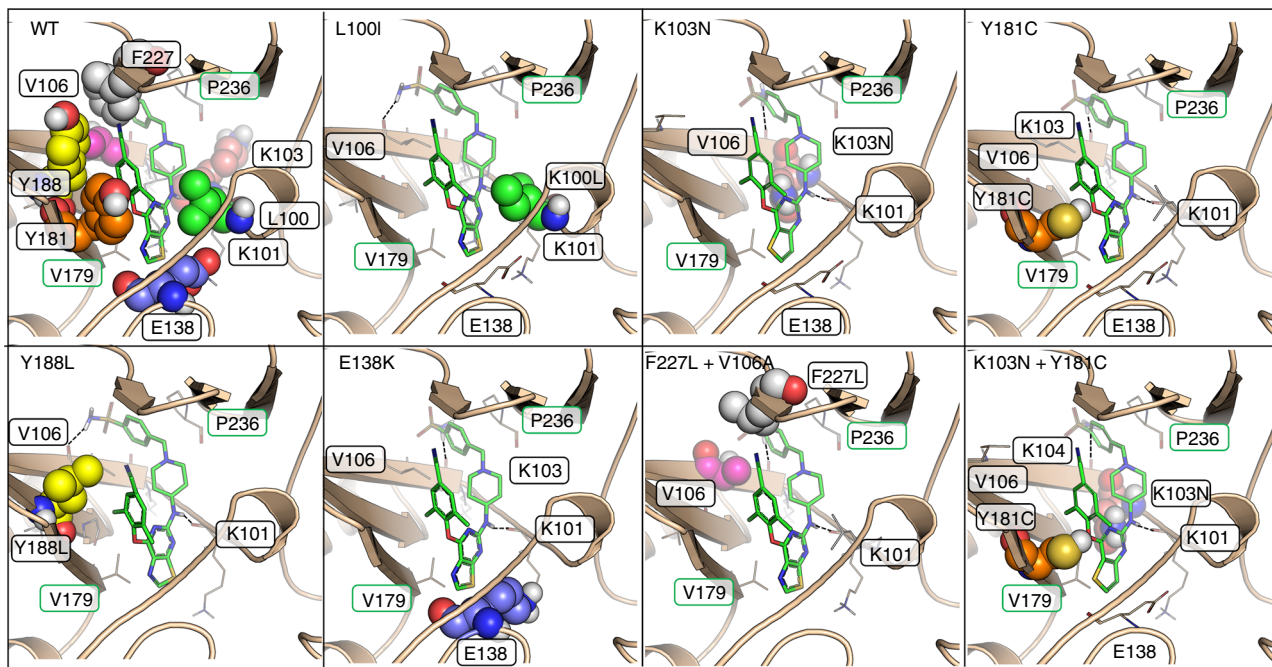
Fig. 3 Molecular modeling studies. Comparison of binding mode of ETV (pink stick), **K-5a2** (cyan stick) and **19a** (green stick) is shown in the NNIBP and the clinically relevant mutants are shown in spheres. Binding mode of **19a** in WT and various mutants is shown and its key intercations are highlighted (residues which form hydrogen bonding and hydrophobic interactions are shown in black and green boxes)

Table 4 Physicochemical parameters of the preferred compounds

Compounds	Aqueous solubility (µg/mL)[a]			Log P[b]	LE[c]	LLE[d]	LELP[e]
	pH 7.4	pH 7.0	pH 2.0				
14a	<1	2.52	197.3	3.04	0.31	5.62	9.78
14c	10.3	20.4	>200	3.21	0.31	5.45	10.3
14d	33.8	30.7	192.9	3.44	0.35	5.30	9.81
19a	3.52	9.94	178.3	3.04	0.32	5.76	9.63
19b	3.11	8.35	180.2	3.45	0.32	5.35	10.6
19c	4.76	15.0	>200	3.21	0.33	5.43	9.72
19d	9.24	32.4	>200	3.44	0.34	5.13	10.0
K-5a2	«1	0.05	189.6	4.46	0.31	4.39	14.2
ETV	<1	<1	126.8	4.19	0.40	4.10	10.4

[a]Measured with HPLC method
[b]Predicted by ACS/Lab 6.0 software
[c]Calculated by the formula $-\Delta G/HA$ (nonhydrogen atom), in which normalizing binding energy $\Delta G = -RT \ln K_d$, presuming $K_d \approx EC_{50 \ (IIIB)}$
[d]Calculated by the formula $pEC_{50} - \log P$
[e]Calculated by the formula $\log P/LE$

bioavailability (F) for a drug candidate, and the oral bioavailability of **19a** up to 83.8%.

Safety assessment. We evaluated the acute toxicity of **14a** and **19a** in Kunming mice. After oral gavage administrations with a dose of 2000 mg/kg, there was no death and no abnormity of body weight change compared to control group in the following one week (Supplementary Fig. 6). The results support the great potential of **14a** and **19a** as novel NNRTI drug candidates with low acute toxicity.

The subacute toxicity experiments of **14a** and **19a** were carried out to further evaluate their in vivo safety. No apparent signs associated with animal toxicity and no behavioral abnormalities were observed during the treatment period of po administered

mice treated with 50 mg/kg of **14a** and **19a** every day for 7 days. Furthermore, hematoxylin and eosin (H&E) staining was utilized for histological analysis of the major organs. As displayed in Fig. 4, no apparent physiological abnormalities or lesions were observed in the heart, liver, spleen, lungs, and kidneys, suggesting the negligible side toxicity of **14a** and **19a**.

Compounds with a high affinity for the hERG potassium channel could induce QT interval prolongation, which is frequently related to potentially risk for cardiotoxicity[23]. So we next evaluated their hERG inhibition activity, and Terfenadine was selected as reference drug (Supplementary Tables 3, 4). As shown in Supplementary Figs. 7, **14a** and **19a** showed an IC_{50} of 0.18 and 0.12 µM against the potassium channel respectively. Although the IC_{50} values indicated that **14a** and **19a** has a risk of

cardiotoxicity, their hERG inhibition activity lower than that of terfenadine ($IC_{50} = 0.022\,\mu M$)[9], which gave us much confidence for the further development.

Discussion

Although second-generation NNRTIs achieved success in suppressing HIV-1 replication and reducing viral loads, poor aqueous solubility, dose-limiting toxicity, and the rapid generation of drug-resistant mutations in HIV-1 RT remains a major impediment to effective anti-HIV treatment. The application of structural mimics of a range of scaffolds or peripheral substituents, commonly designated as bioisosteres, is a common approach in contemporary drug design and discovery. With ETV as a lead, two piperidine-substituted thiophene[3,2-*d*]pyrimidine derivatives, **K-5a2** and **25a**, with potent activity against WT and mutant HIV-1 strains were recently discovered as drug candidates in our lab. However, both of them encountered some deficiency, including weak activity against RES056 (**K-5a2**), higher cytotoxicity (**25a**) and low bioavailability (**K-5a2** and **25a**), so there still is an urgent need for searching novel NNRTIs with improved antiviral potency against WT HIV and mutant strains, reduced adverse effects and more favorable pharmacokinetic profiles.

In current study, with **K-5a2** as lead, series of anti-HIV compounds were designed and synthesized guided by structural biology studies and bioisosteric replacement strategy. Especially, we detailed the results of our efforts to optimize the in vivo and in vitro properties of derivatives prepared from the furo[3,2-*d*]pyrimidine, thiazolo[4,5-*d*]pyrimidine and thiazolo[5,4-*d*]pyrimidine core. The results of in vitro assay of anti-HIV activities demonstrated that most of the synthesized compounds showed more active potency than ETV. In the case of RT variants bearing prevalent drug-resistant mutations, compounds with thiazolo[4,5-*d*]pyrimidine and thiazolo[5,4-*d*]pyrimidine core also displayed greater potency than ETV, such as **14a**, **14c**, and **19a–c**. The SARs could be concluded that hydrophilic substituents harboring hydrogen bond donors or acceptors ($-SO_2NH_2$, $-CONH_2$, and $-SO_2CH_3$) can significantly improve drug resistance profiles.

Moreover, the selected potent compounds exhibited an IC_{50} values of 0.037–0.050 μM in the recombinant HIV-1 RT enzyme assays and confirmed the binding target of these compounds is RT. Molecular modeling studies illustrate the molecular details of the binding poses of **19a**, extensive hydrophobic interactions and network of main chain hydrogen bonds formed between the NNRTIs and NNIBP, and provide reasonable explanation for the improved drug resistance profiles, which give an effective evidence that the NNRTIs could retain effective activities against mutant HIV-1 strains by taking advantage of the structural flexibility of the inhibitors, plasticity of the NNIBP and the hydrogen bonding between the NNRTIs and the main chains of NNIBP residues.

Furthermore, **14a** and **19a** were identified as promising hit compounds after screening of compounds solubility, ligand efficiency calculations, and CYP enzymatic inhibition activity. Especially, **19a** with favorable pharmacokinetic properties and its bioavailability reaches up to 83.8%. Moreover, both compounds showed good safety profiles, including acute toxicity, subacute toxicity and cardiotoxicity. In conclusion, the current study confirmed a potential anti-HIV-1 drug candidate with improved drug resistance profiles and favorable druggability, and the preclinical studies are under way.

Methods

Synthetic procedures. See Supplementary Methods and Supplementary Figs. 1, 2. For NMR spectra see Supplementary Figs. 8–16.

Anti-HIV activity test studies. See Supplementary Methods and Supplementary Table 1.

HIV-1 RT inhibitory assays and cytochrome P450 inhibition assay. See Supplementary Methods

---

Table 5 The CYP enzymatic inhibitory activity of the selected lead compounds

CYP isozyme	Standard inhibitor	IC₅₀ (μM)	IC₅₀ (μM)		
			14a	**19a**	**19c**
1A2	α-Naphthoflavone	0.311	>50.0	>50.0	>50.0
2C9	Sulfaphenazole	0.643	13.2	6.91	4.43
2C19	(+)-*N*-3-benzylnirvanol	0.259	21.2	18.2	19.1
2D6	Quinidine	0.158	15.2	38.6	34.1
3A4M	Ketoconazole	0.0433	5.92	3.73	2.78
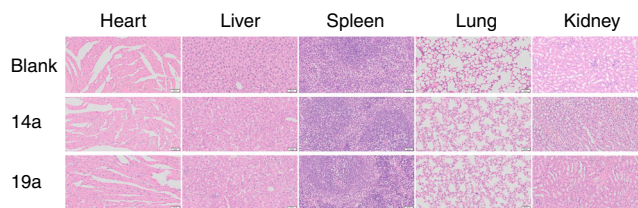
Fig. 4 The result of subacute toxicity. H&E stained images of major organs (heart, liver, spleen, lung, and kidney) collected from various groups (blank, **14a** and **19a**). The scale bar was 50 μm

---

Table 6 Pharmacokinetic profile of 14a and 19a

Subject	$T_{1/2}$ (h)	T_{max} (h)	C_{max} (ng/mL)	AUC_{0-t} (h*ng/mL)	$AUC_{0-\infty}$ (h*ng/mL)	CL (L/h/kg)	F (%)
14a (iv)[a]	2.01 ± 1.3	0.033	—	231 ± 112	234 ± 114	10.2 ± 3.8	—
14a (po)[b]	3.12 ± 0.6	0.90 ± 0.7	272 ± 77	1063 ± 283	1082 ± 262	—	45.9
19a (iv)[a]	0.93 ± 0.3	0.033	—	118 ± 6.7	123 ± 10.4	16.3 ± 1.2	—
19a (po)[b]	2.0 ± 0.8	2.8 ± 1.1	2982 ± 257	993 ± 301	1023 ± 301	—	83.8
K-5a2 (iv)[a]	1.61 ± 0.3	0.033	—	2949 ± 2870	3118 ± 3159	1.01 ± 0.48	-
K-5a2 (po)[b]	3.21 ± 0.7	0.9 ± 0.2	1626 ± 584	6752 ± 3099	7349 ± 3454	—	22.9

PK parameters (mean ± SD, $n = 5$)
[a]Dosed intravenously at 2 mg/kg
[b]Dosed orally at 20 mg/kg

Molecular modeling methods. See Supplementary Methods, Supplementary Table 2, and Supplementary Tables 3, 4.

Pharmacokinetics assays and acute toxicity experiment. See Supplementary Methods and Supplementary Figs. 5, 6

hERG activity assay procedures. See Supplementary Methods, Supplementary Tables 3, 4, and Supplementary Fig. 7

Laboratory animals. The authors declare that all experimental work complied with the institutional guidelines on animal studies (care and use of laboratory animals).

Data availability
The authors declare that the data supporting the findings of this study are available within the paper and its supplementary information.

References
1. Bec, G. et al. Thermodynamics of HIV-1 reverse transcriptase in action elucidates the mechanism of action of non-nucleoside inhibitors. *J. Am. Chem. Soc.* **135**, 9743–9752 (2013).
2. Zhan, P., Pannecouque, C., De Clercq, E. & Liu, X. Anti-HIV drug discovery and development: current innovations and future trends. *J. Med. Chem.* **59**, 2849–2878 (2016).
3. Wainberg, M. A., Zaharatos, G. J. & Brenner, B. G. Development of antiretroviral drug resistance. *New Engl. J. Med.* **365**, 637–646 (2011).
4. Lehman, D. A. et al. Low-frequency nevirapine resistance at multiple sites may predict treatment failure in infants on nevirapine-based treatment. *J. Acquir. immune Defic. Syndr.* **60**, 225–233 (2012).
5. Beyrer, C. & Pozniak, A. HIV drug resistance - an emerging threat to epidemic control. *New Engl. J. Med.* **377**, 1605–1607 (2017).
6. Namasivayam, V. et al. The journey of HIV-1 non-nucleoside reverse transcriptase inhibitors (NNRTIs) from lab to clinic. *J. Med. Chem.* **62**, 4851–4883 (2018).
7. Wu, P. Y. et al. Multicenter study of skin rashes and hepatotoxicity in antiretroviral-naive HIV-positive patients receiving non-nucleoside reverse-transcriptase inhibitor plus nucleoside reverse-transcriptase inhibitors in Taiwan. *PLoS ONE* **12**, e0171596 (2017).
8. Kang, D. et al. Design, synthesis, and evaluation of thiophene[3,2-d]pyrimidine derivatives as HIV-1 non-nucleoside reverse transcriptase inhibitors with significantly improved drug resistance profiles. *J. Med. Chem.* **59**, 7991–8007 (2016).
9. Kang, D. et al. Structure-based optimization of thiophene[3,2-d]pyrimidine derivatives as potent HIV-1 non-nucleoside reverse transcriptase inhibitors with improved potency against resistance-associated variants. *J. Med. Chem.* **60**, 4424–4443 (2017).
10. Lee, W. G. et al. Picomolar inhibitors of HIV reverse transcriptase featuring bicyclic replacement of a cyanovinylphenyl group. *J. Am. Chem. Soc.* **135**, 16705–16713 (2013).
11. Zhang, S. et al. Efficient drug discovery by rational lead hybridization based on crystallographic overlay. *Drug Disco. Today* **24**, 805–813 (2018).
12. Pennington, L. D. & Moustakas, D. T. The necessary nitrogen atom: a versatile high-impact design element for multiparameter optimization. *J. Med. Chem.* **60**, 3552–3579 (2017).
13. Dagmar, S., Ye, H., Dilyana, D. & Jürgen, B. Recent progress in understanding activity cliffs and their utility in medicinal chemistry. *J. Med. Chem.* **57**, 18–28 (2014).
14. Stumpfe, D. & Bajorath, J. Exploring activity cliffs in medicinal chemistry. *J. Med. Chem.* **55**, 2932–2942 (2012).
15. Yang, Y. et al. Structural basis for potent and broad inhibition of HIV-1 RT by thiophene[3,2-d]pyrimidine non-nucleoside inhibitors. *eLife* **7**, e36340 (2018).
16. Schafer, W. et al. Non-nucleoside inhibitors of HIV-1 reverse transcriptase: molecular modeling and X-ray structure investigations. *J. Med. Chem.* **36**, 726–732 (1993).
17. Freeman-Cook, K. D., Hoffman, R. L. & Johnson, T. W. Lipophilic efficiency: the most important efficiency metric in medicinal chemistry. *Future Med. Chem.* **5**, 113–115 (2013).
18. Tarcsay, A., Nyiri, K. & Keseru, G. M. Impact of lipophilic efficiency on compound quality. *J. Med. Chem.* **55**, 1252–1260 (2012).
19. Lynch, T. & Price, A. The effect of cytochrome P450 metabolism on drug response, interactions, and adverse effects. *Am. Fam. physician* **76**, 391–396 (2007).
20. Isoherranen, N., Kunze, K. L., Allen, K. E., Nelson, W. L. & Thummel, K. E. Role of itraconazole metabolites in CYP3A4 inhibition. *Drug Metab. Dispos.: Biol. fate Chem.* **32**, 1121–1131 (2004).
21. Kanayama, N., Kanari, C., Masuda, Y., Ohmori, S. & Ooie, T. Drug-drug interactions in the metabolism of imidafenacin: role of the human cytochrome P450 enzymes and UDP-glucuronic acid transferases, and potential of imidafenacin to inhibit human cytochrome P450 enzymes. *Xenobiotica; Fate Foreign Compd. Biol. Syst.* **37**, 139–154 (2007).
22. Guengerich, F. P. Cytochrome P-450 3A4: regulation and role in drug metabolism. *Annu. Rev. Pharmacol. Toxicol.* **39**, 1–17 (1999).
23. Vandenberg, J. I. et al. hERG K(+) channels: structure, function, and clinical significance. *Physiol. Rev.* **92**, 1393–1478 (2012).

Author contributions
D.K., C.P., P.Z., and X.L. conceived the project. D.K., Z.W., D.F., H.Z., G.W., F.W., Z.Z., and L.J. finished the compounds synthesis and structure confirmation. D.K., T.Z., and X.Z. designed the pharmacokinetics assays and acute toxicity experiment. D.K. and Z.W. performed the CYP450 inhibition assay. D.K., B.H., and Y.T. performed the data analysis. V.P. and J.K. performed the molecular modeling study. E.D.C. and C.P. performed the evaluation of compounds activity. C.P., P.Z., and X.L. provided the resources, supervision and funding assistance. All authors critically evaluated the manuscript prior to submission.

Additional information
Supplementary information accompanies this paper at https://doi.org/10.1038/s42004-019-0174-8.

Competing interests: The authors declare no competing interests.

Reprints and permission information is available online at http://npg.nature.com/reprintsandpermissions/

Publisher's note: Springer Nature remains neutral with regard to jurisdictional claims in published maps and institutional affiliations.